

Mixing and flushing in the Persian Gulf (Arabian Gulf)

Yousef Alosairi,¹ Jörg Imberger,² and Roger A. Falconer¹

Received 27 October 2010; revised 25 December 2010; accepted 18 January 2011; published 31 March 2011.

[1] The assimilative capacities of estuaries and coastal seas for effluent discharges are predominantly determined by the rates at which pollutant-bearing effluents are first dispersed and then flushed from the coastal region into the open ocean. The dispersion coefficients and flushing, as measured by the water residence time in the Persian Gulf (Arabian Gulf), were investigated using the three-dimensional numerical model Estuary, Lake and Coastal Ocean Model (ELCOM). The model was first validated using the R/V *Mt. Mitchell* expedition profile data, collected from 27 January to 26 February 1992 and from 13 May to 12 June 1992. The validated model was then used to compute the geographic variability of the horizontal dispersion coefficients K_x throughout the gulf. Model results revealed that dispersion was principally driven by the shear associated with the tides, but along the Arabian coast, wind was an additional significant energy source for dispersion. The water residence time was found to be more than 3 years along the Arabian coast, but shorter along the Iranian coast.

Citation: Alosairi, Y., J. Imberger, and R. A. Falconer (2011), Mixing and flushing in the Persian Gulf (Arabian Gulf), *J. Geophys. Res.*, 116, C03029, doi:10.1029/2010JC006769.

1. Introduction

[2] The Persian Gulf (Arabian Gulf, hereinafter called the gulf), shown in Figure 1, is a relatively shallow coastal basin that extends between 22° and 30° north and between 48° and 56° east and is surrounded by eight countries, namely: Kuwait, Saudi Arabia, Bahrain, Qatar, United Arab Emirates, Oman, Iran and Iraq. The gulf has a maximum width of 338 km, a length of about 1000 km, a mean depth of 36 m and a volume of around 900 km³. It is separated from the Gulf of Oman by the Strait of Hormuz which, at its narrowest point is only 56 km wide. From the strait seaward toward the Indian Ocean the depth gradually increases from 100 m to 2000 m. River inflows occur mostly in the northern end of the gulf, primarily on the Iranian side, with the largest being the Shatt Al Arab—a river formed by convergence of the Tigris, Euphrates, and Karun rivers (Figure 1). This river has an average annual flow of around 1456 m³/s. Other key rivers are the Hendijan (203 m³/s), the Hilleh (444 m³/s), and the Mand (1387 m³/s) (see Figure 1) [Reynolds, 1993].

[3] The gulf is generally bowl-shaped, with very shallow depths along the Arabian coastline, with particularly shallow waters occurring around the western coastline adjacent to Kuwait, Qatar, and United Arab Emirates, ranging from 10 to 15 m. Rapid coastal development in these gulf countries has caused considerable ecological stress in the shallow

coastal regions, with increasing levels of effluent discharges from oil production, exploration and transportation, as well as from municipal and petrochemical activities, and red tides having been noted along various parts of the Arabian coast [Richlen *et al.*, 2010].

[4] Traditionally, coastal communities have relied on dispersion of effluents once they entered coastal waters so that, once diluted, biological breakdown has rendered them harmless. Here we define the “assimilative capacity” as that loading, which properly dispersed throughout the receiving domain, can be rendered harmless without jeopardizing the health of the ecosystem. Clearly, three distinct sets of processes combine to determine whether a domain has the assimilative capacity to accept an additional effluent loading. First, the near and intermediate rates of dispersal must be sufficiently fast to dilute the effluent to a level sufficiently low, that when added to the background concentration, it does not kill components of the ecosystem impacting on the functioning of the ecosystem [Imberger *et al.*, 2007]. Second, the transport or flushing must remove the by-products of the effluent breakdown processes sufficiently rapidly such that there is no long-term build up in the domain as a whole. In simple terms the flushing must prevent the domain from filling up with harmful products, implying that the criterion of whether a discharge is acceptable or not may depend on an event in the future. Third, the ecosystem must have the biochemical capacity necessary to ensure the breakdown of those pollutants that may be harmful to the rest of the original food chain. In the present paper we concern ourselves with only the first two, the physics of dispersion and flushing in the gulf. In particular, our objective is to determine the geographic dispersion and flushing characteristics of the gulf, in terms of residence time, to provide

¹Cardiff School of Engineering, Cardiff University, Cardiff, UK.

²Centre for Water Research, University of Western Australia, Crawley, Western Australia, Australia.

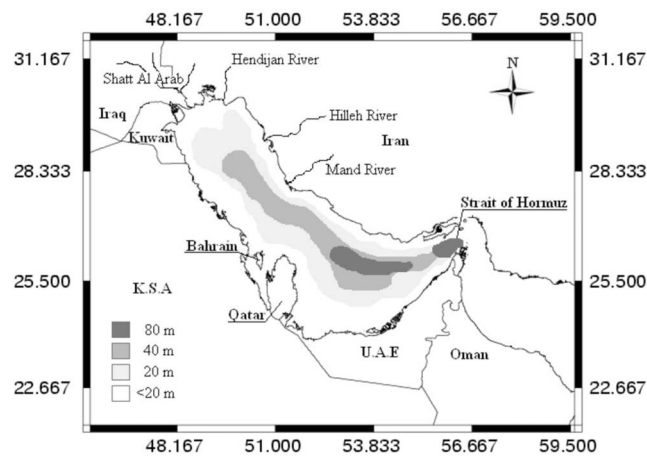


Figure 1. Persian Gulf (Arabian Gulf) physical characteristics. Source: National Geophysical Data Centre (<http://www.ngdc.noaa.gov>).

a guide for new engineering developments and their environmental management.

2. Horizontal Dispersion Mechanisms

2.1. Mixing Regimes

[5] Dispersion is achieved by the following three mechanisms [Fischer *et al.*, 1979]:

[6] 1. Turbulent near field dispersion, where the dispersion is energized by the turbulent kinetic energy from the discharge itself.

[7] 2. The region following the near field, called the intermediate field, where the mixing switches from being discharge energized to mixing that is energized by the turbulence of the ambient fluid flow. When the effluent density differs from that of the receiving water, the intermediate region can be quite significant in extent because the added buoyancy must be overcome by energy from the receiving water flow.

[8] 3. The far field, where the pollutant is dispersed by mechanisms inherent in the ambient flow conditions.

2.2. Far Field Mixing

2.2.1. Turbulent Dispersion

[9] After initial dispersion in the near field, effluents disperse by turbulent mixing until the effluent cloud has reached a size comparable to the scale of the velocity field. Once it is as large as the scale of the shear, the mean background velocity field distorts the effluent cloud and shear and transverse mixing combine to yield an enhanced dispersion (see section 2.2.2). For effluent clouds smaller than the scale of the background shear, turbulence disperses the effluent cloud and Richardson [1926] showed that the dispersion may be modeled by the “4/3 law,” which accounts for the rate of increase of dispersion as the effluent cloud intersects ever increasing scales of turbulence as the cloud grows.

2.2.2. Shear Dispersion

[10] Longitudinal shear dispersion occurs when the distortion of a concentration field by a vertical or horizontal

shear flow is balanced by vertical or transverse turbulent mixing [Fischer *et al.*, 1979]. Once balance is achieved the rate of dispersion may be modeled [see Fischer *et al.*, 1979] by a simple diffusion equation with a horizontal dispersion coefficient

$$K_x = \phi \frac{U^2 l^2}{K_z}$$

Here ϕ is a constant dependent on the velocity and transverse diffusivity profile, l is the length scale of the velocity straining the concentration field, U is the velocity scale and K_z is the vertical diffusivity. As demonstrated by Fischer *et al.* [1979] for a simple plane flow with a vertical turbulent velocity profile, $l = h$, where h is the depth, U is the discharge velocity, and $K_z = 0.07hU^*$, where U^* is the bottom shear velocity. By contrast, in a wide river with a transverse velocity profile, l becomes the width of the channel and U is the discharge velocity. The coefficient ϕ depends on the vertical structure of the velocity and diffusivity. For constant diffusivity, Fischer *et al.* [1979] showed that $\phi = 0.008$ for a linear velocity profile and Bowden [1965] showed that $\phi = 0.001$ for a logarithmic profile resulting from bottom friction, $\phi = 0.019$ for the density current profile, and $\phi = 0.005$ – 0.008 for wind drift profiles.

[11] Clearly, dispersion due to the balance of transverse mixing and longitudinal straining will always be much larger than that due to vertical mixing in shallow estuaries. However, the validity of this statement depends on the time available for mixing. It is well known [see Fischer *et al.*, 1979] that a balance between distortion due to velocity shear and that due to transverse mixing can be achieved only after there has been sufficient time for transverse mixing to take place, a time of $O\left(\frac{l^2}{K}\right)$ where K is the horizontal (or vertical) diffusion coefficient. Shear dispersion via vertical shear with, typically a depth of 10 m and a vertical diffusion coefficient of around 10^{-4} m²/s leads to a set up time $O(12)$ days and a horizontal dispersion coefficient of around 6 m²/s, assuming a value of $\phi = 0.01$ and $U = 0.025$ m/s. If the water velocity is around 0.5 m/s, then shear dispersion would become relevant only after 500 km, which is already half of the studied domain. By contrast, if we assume a coastal current with a transverse scale of 1 km and a transverse diffusion coefficient of 1 m²/s, then the horizontal dispersion coefficient for transverse mixing and longitudinal strain balance would be around 2500 m²/s and the time required to reach such a balance would again be $O(12)$ days. So we see that the larger the length scale, the larger the horizontal dispersion. However, again the distance required for this estimate to become valid would be comparable to, or larger than, the dimensions of the gulf itself [Lewis, 1997; Dooley and Steele, 1969].

[12] Dispersion of a coastal effluent discharge occurs in several stages. First, in the near field the mean kinetic energy of the discharge generates turbulence that mixes or stirs the discharge into the receiving water. Second, in the absence of a buoyancy flux the diluted effluent is mixed with the receiving water turbulence until the cloud reaches a scale comparable to the scale of the ambient velocity field. Once this happens the mean velocity shear distorts the cloud, rather than simply transporting it, and this distortion

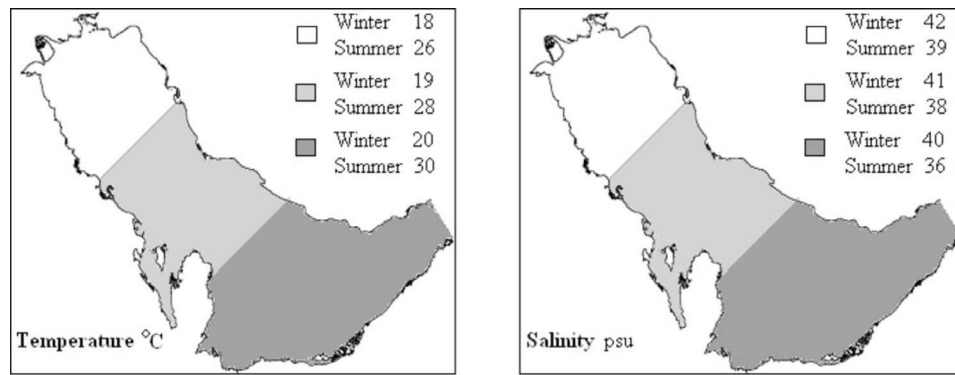


Figure 2. Initial condition configurations of temperature and salinity in ELCOM during winter and summer.

may interact with the ambient turbulent mixing to produce shear dispersion and/or stagnation point dispersion as with *Okely et al.* [2010], or it may interact with particular kinematic flow forms to produce kinematic chaos or ghost rod dispersion [Aref, 1984; Stocker and Imberger, 2003; Boyland et al., 2000; Newhouse and Pignataro, 1993]. Although the last three forms of dispersion were not specifically investigated in the present study, as this would require an extensive field survey to identify individual processes, it is likely that each contributes to the dispersion evaluated numerically with the 3-D model.

[13] Here we first validate a 3-D model of the flow dispersion in the gulf by showing that the model reproduces the dispersion of the salinity field originating from the Strait of Hormuz and river inflows. The salinity differences were low enough not to influence the buoyancy, with salinity acting simply as a tracer in the upper reaches of the gulf. Once validated, the 3-D model was used to ascertain the degree of dispersion of tracers as a function of geographic location, the processes sustaining the simulated dispersion and the net flushing or residence time resulting from this dispersion.

3. ELCOM

3.1. Brief Description of Model

[14] The Estuary Lake Coastal Ocean Model (ELCOM) applied to the gulf solves the 3-D, hydrostatic, Boussinesq, Reynolds-averaged Navier-Stokes, and scalar transport equations, to model velocity, temperature and salinity distributions in space and time [Hodges et al., 2000]. The model utilizes a fixed, Z coordinate finite difference mesh with Euler-Lagrangian approach for momentum advection, Ultimate-Quickest scheme for advection of scalars and a kinematic boundary condition for the free surface evolution [Casulli and Cheng, 1992; Leonard, 1991; Casulli and Cattani, 1994]. Scalars and momentum are mixed vertically according to the excess of turbulent kinetic energy available from wind stirring and shear production throughout the water column over the potential energy inherent in the ambient stratification [Spigel et al., 1986; Laval et al., 2003]. A new component to allow for tidal generation as a body force was incorporated in the model, necessary because of the relatively long length of the gulf, associated

with a lunar semidiurnal tidal response and its effect in dispersing tracers. Following *Cartwright and Tayler* [1971], tidal forces were calculated from the gravitational potential and included in the momentum-transport equation in ELCOM.

3.2. Model Setup

[15] The modeling approach adopted in this study involved a uniform grid of 5000 m in both X and Y directions. Twenty layers in the Z direction at increments of 4 m for the first top 11 layers and 4.5 m for the remaining layers were adopted leading to a total of 104,056 wet cells discretizing the domain, and a Neumann boundary condition was applied at the open boundary. A computational time step of 300 s was utilized in the model. The bathymetric information was obtained from a map digitiser at the Hydro-Environmental Research Centre of Cardiff University that interpolated the depth at each grid point from a map obtained from the United Kingdom Hydrographic Office. The sea surface elevation due to semidiurnal tide is prescribed at the open boundary at the Strait of Hormuz using the KGULF model developed by Al-Salem (Kuwait Institute of Scientific Research, 2009) for the 1992 period (available on Coastal Information System www.hceatkuwait.net). The salinity and temperature data acquired by the R/V *Mt. Mitchell* cruise [Reynolds, 1993] were used as initial conditions for the model. Also, temperature-salinity data gathered in a recent study in the southern part of the gulf [Elshorbagy et al., 2006] were used to define three main subdomains for the model initial conditions, as shown in Figure 2. Discharges from the rivers were assumed to remain constant throughout the simulation, based on the values given by Reynolds [1993], and as explained in the introduction. Horizontal diffusivity, κ , is an input parameter in Estuary, Lake and Coastal Ocean Model (ELCOM) representing turbulent sub grid diffusion in the model transport equations (more details provided by Hodges et al. [2000]) and was set to $1 \text{ m}^2/\text{s}$, but the effect of 5 and $10 \text{ m}^2/\text{s}$ on the horizontal dispersion of numerical tracers was also investigated, as described in section 5 and discussed in section 6. A bottom drag coefficient of 0.005 was assigned to the whole domain to take account of bed friction. A light extinction coefficient of 0.25 was used for light attenuation.

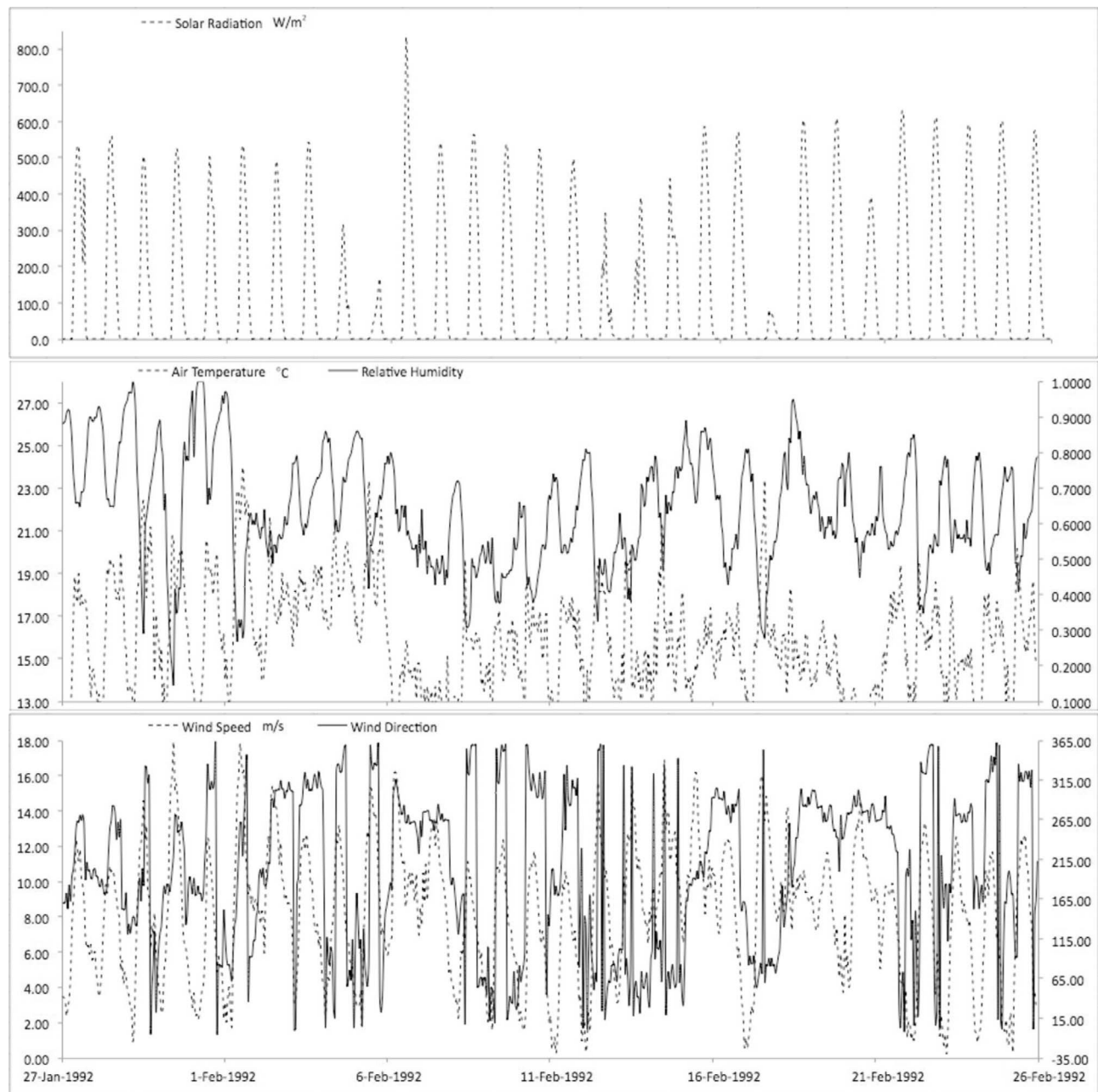


Figure 3. Winter meteorological conditions.

Meteorological forcing, shown in Figures 3 and 4, was applied at 8 m above sea level.

4. Model Validation Using 1992 Field Data

4.1. Meteorological Data

[16] Meteorological effects over the estuary during 1992 were included in the model and were obtained from the Dubai Meteorological Services (DMS), located at the far south of the gulf in Dubai and the Kuwait Institute for Scientific Research (KISR), located at the far north of the gulf, near Kuwait Bay. The differences in meteorological parameters outlined in Figures 3 and 4 between the stations

were insignificant from 27 January to 26 February 1992 and from 13 May to 7 June 1992, in particular for wind speeds as shown in Figures 5 and 6. Not surprisingly, other parameters such as air temperature are seen to vary seasonally at both stations, with values ranging from 15 to 40°C in winter and summer, respectively. Humidity variations were similar to air temperature variations, but in the opposite sense (see Figures 3 and 4) at both stations. Records of solar radiation at both stations showed the same maximum mean values of 550 w/m² during January and February 1992 and 900 w/m² during May and June 1992, probably as a result of the similar geographic locations of the two stations. KISR data for 1992 (Figures 3 and 4) were assumed to be adequate for

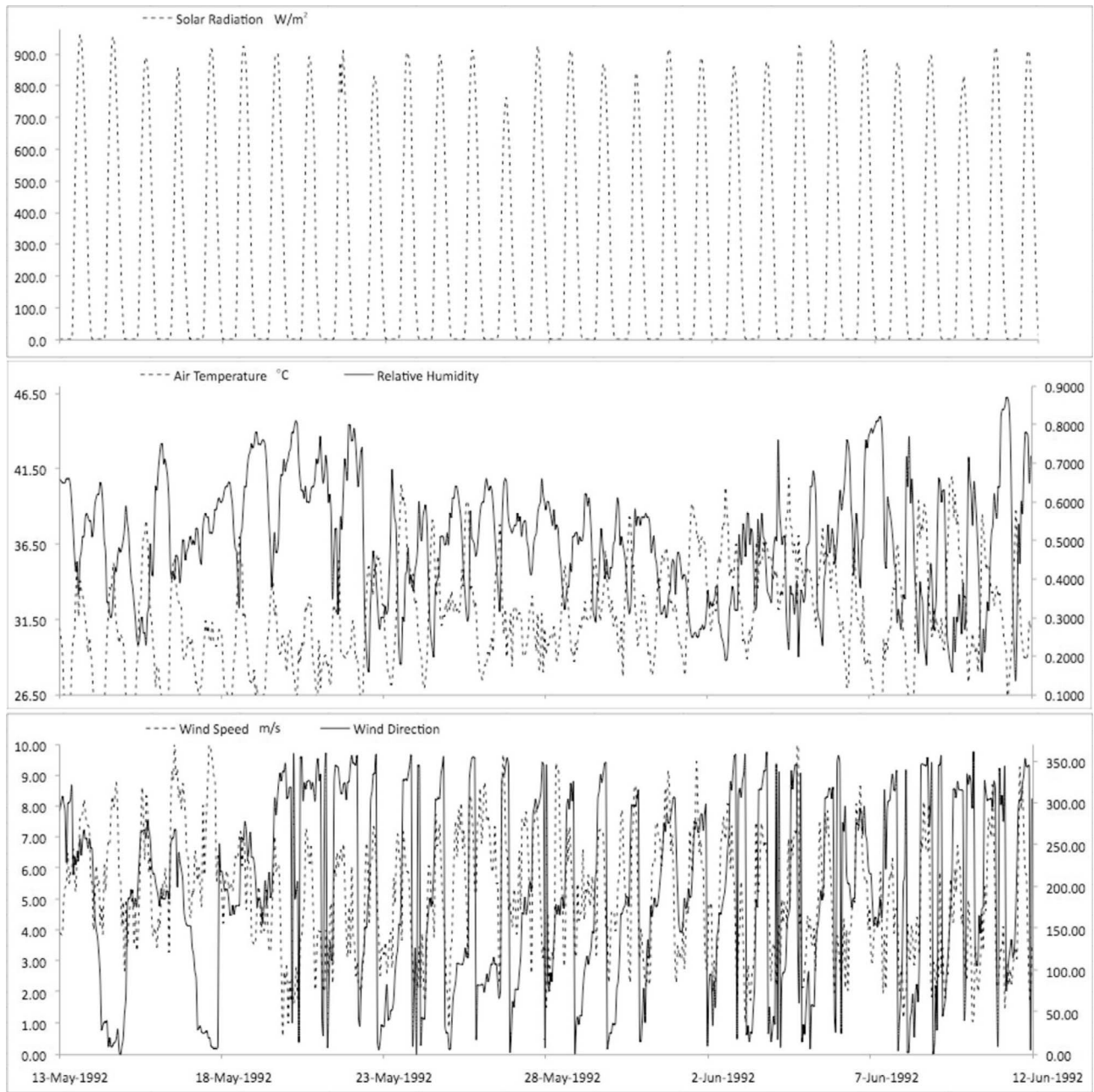


Figure 4. Summer meteorological conditions.

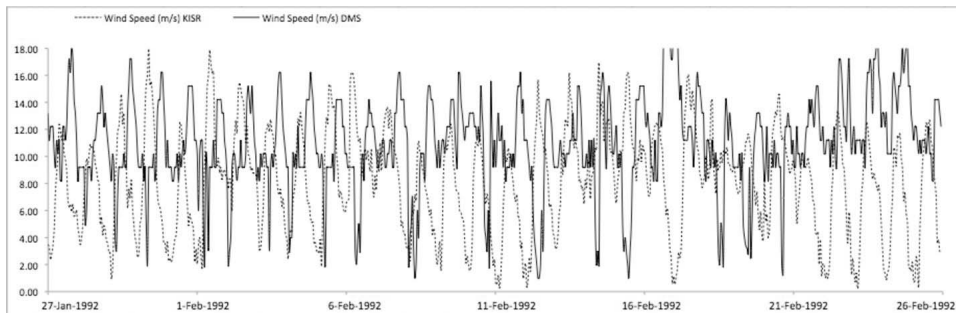


Figure 5. Comparison of wind speed between at KISR and DMS in winter.

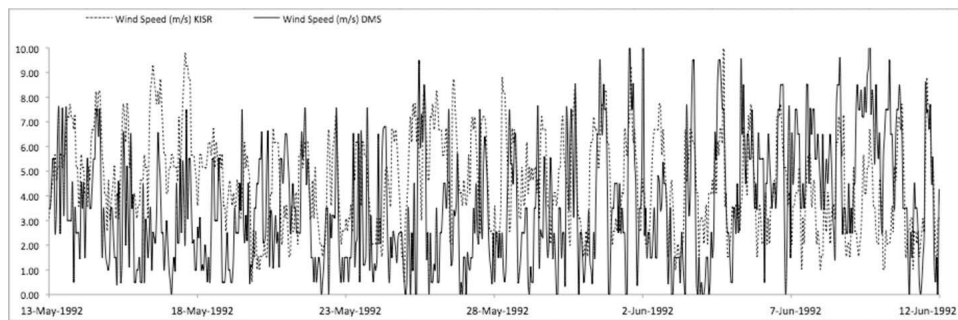


Figure 6. Comparison of wind speed between at KISR and DMS in summer.

our study, as minor differences in meteorological parameters do not have a great influence on the water dynamics of the gulf, which are driven chiefly by the tides [Elshorbagy *et al.*, 2006; Reynolds, 1993].

4.2. Salinity and Temperature in the Gulf

[17] In late 1991 a joint monitoring program was set up by the Regional Organization for the Protection of the Marine Environment (ROPME), the Intergovernmental Oceanographic Commission (IOC) and the National Oceanic and Atmospheric Administration (NOAA) with a vessel supplied by NOAA. A broad, multidisciplinary survey was carried out over six periods for 100 days between February

and June 1992, the relevant results being shown in Figures 7 and 8 [Reynolds, 1992a, 1992b, 1993].

[18] During winter the water column was well mixed vertically to a depth of about 70 m (Figure 7a) and both the temperature and salinity varied gradually along the gulf between Kuwait and the Strait of Hormuz, in which the temperature increased and the salinity decreased toward the strait. Together these variations resulted in a density difference of about 2 kg/m^3 over a distance of 500 km (Figure 7a, bottom). In summer, the surface mixing penetrated to a depth of only about 30 m and the 25°C isotherm (Figure 7b, top) was almost horizontal over the whole domain. More saline and cooler water was observed (Figure 7b, middle), its location between 100 and 700 km southeast Kuwait, sug-

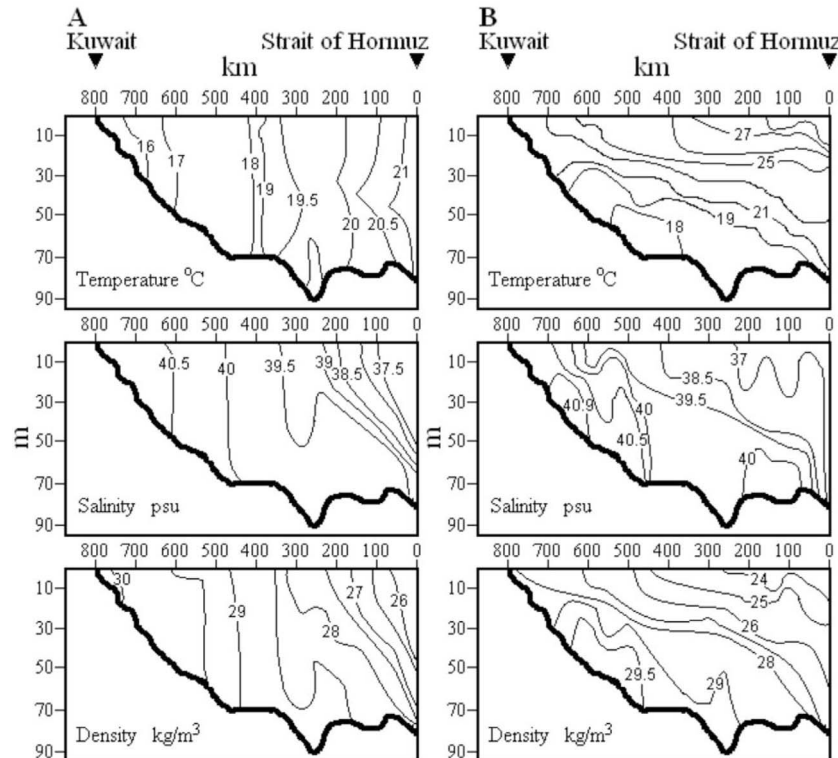


Figure 7. (a) Vertical variation of temperature, salinity, and density along the gulf (from the Strait of Hormuz to Kuwait) during winter; starting 26 February 1992 [Reynolds, 1993]. (b) Vertical variation of temperature, salinity, and density along the gulf (from the Strait of Hormuz to Kuwait) during summer; starting 12 June 1992 [Reynolds, 1993].

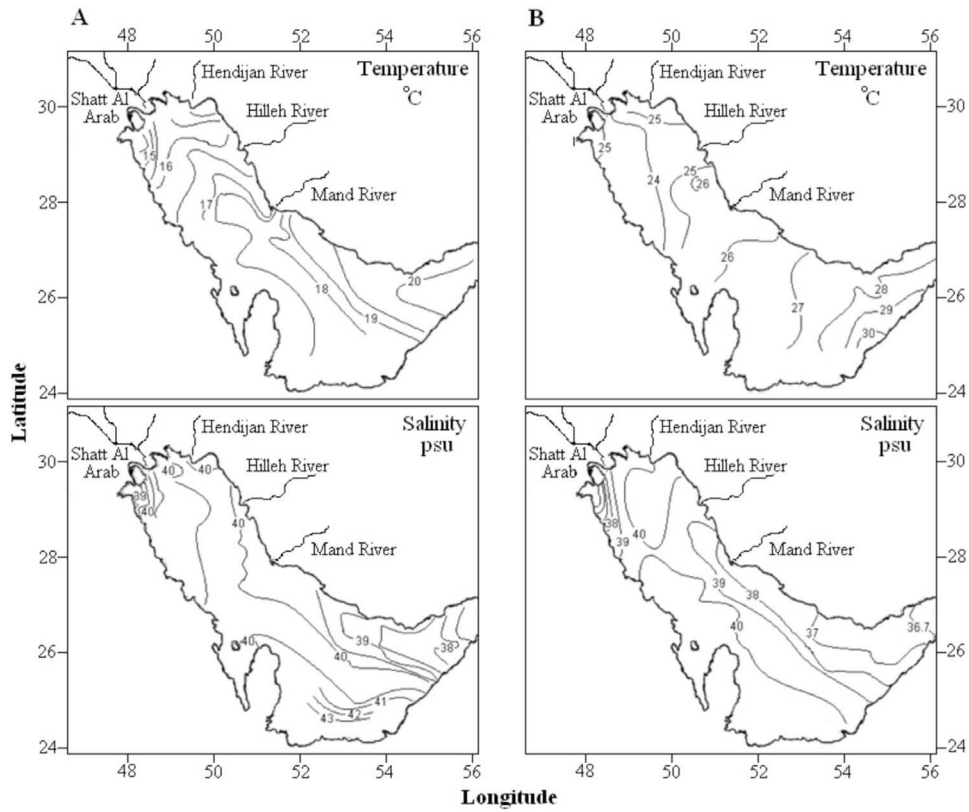


Figure 8. Surface field data variation of temperature and salinity of the gulf during (a) winter, starting 26 February 1992 [Reynolds, 1993], and (b) summer, starting 12 June 1992 [Reynolds, 1993].

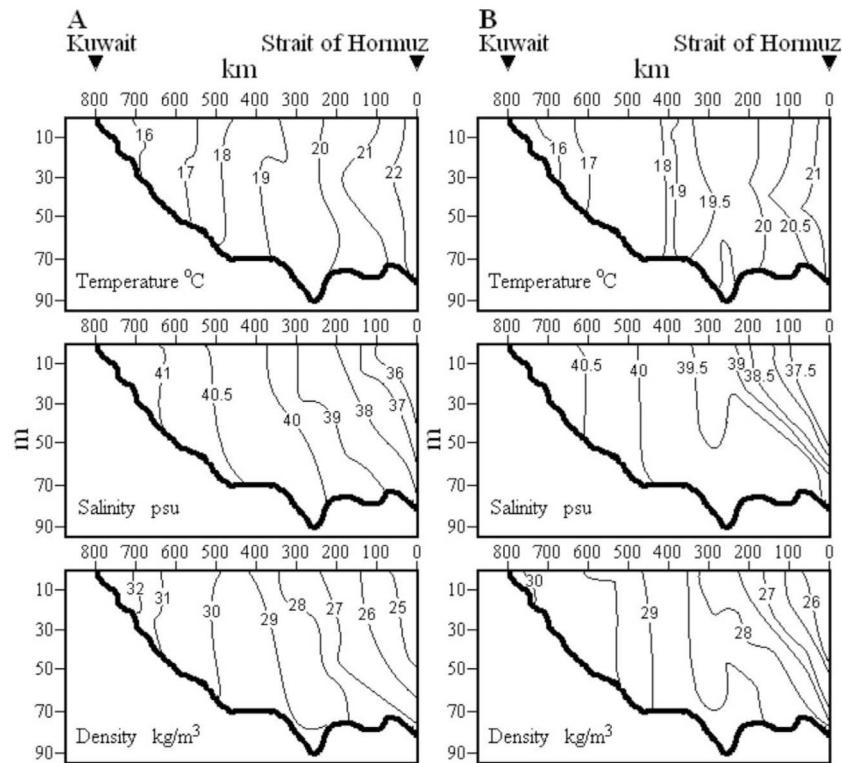


Figure 9. (a) Simulated vertical variation of temperature, salinity, and density along the gulf (from the Strait of Hormuz to Kuwait) during winter (1992). (b) Field data variation of temperature, salinity, and density along the gulf (from the Strait of Hormuz to Kuwait) during winter (1992).

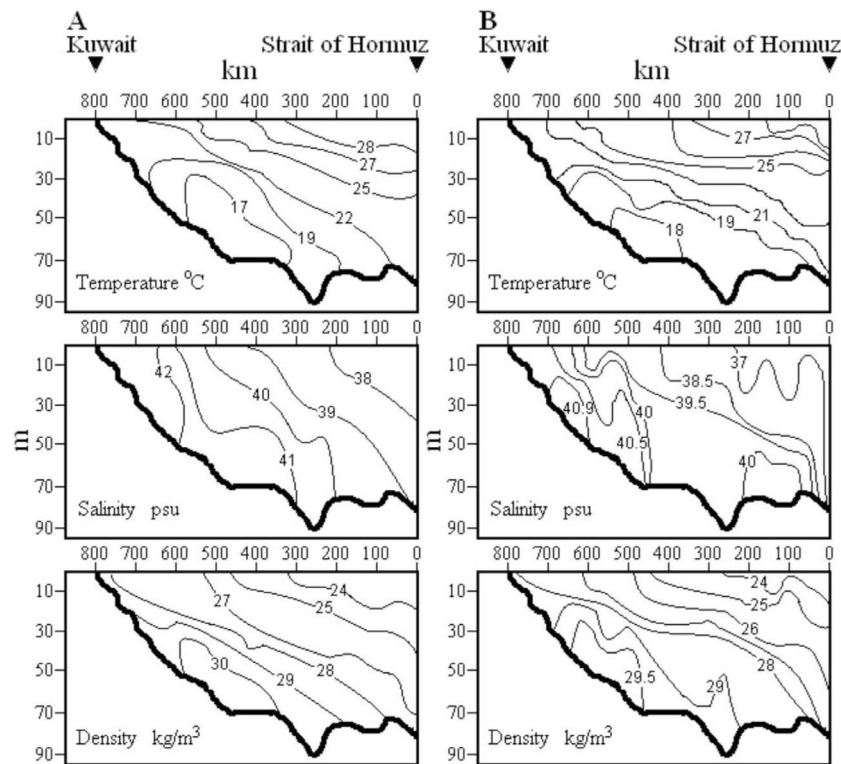


Figure 10. (a) Simulated vertical variation of temperature, salinity, and density along the gulf (from the Strait of Hormuz to Kuwait) during summer (1992). (b) Field data variation of temperature, salinity, and density along the gulf (from the Strait of Hormuz to Kuwait) during summer (1992).

gesting an origin not in the Strait of Hormuz, as the salinity maximum lies over 100 km away from the strait. Furthermore, as seen from Figure 7b (bottom), the isopycnals showed a distinct slope downward toward the strait, the origin of this water column therefore most likely being the gulf perimeter, where evaporation over shallow water would increase salinity. The Strait of Hormuz acts as a hydraulic control for the exchange between the Persian Gulf (Arabian Gulf) and the Gulf of Oman, the upper layer of fresher water transferring from the Gulf of Oman to replace water lost by evaporation, and the lower, higher saline water exiting to complete the reverse estuarine circulation [Reynolds, 1993]. More details of the temperature, salinity and density cross sections across the estuary between Kuwait and Iran, Qatar and Iran, and across the Strait of Hormuz are given by Reynolds [1993]. The surface inflow from the Gulf of Oman into the Persian Gulf (Arabian Gulf) occurs year-round, but extends deeper along the northern boundary into the gulf in the summer, as seen in Figures 7 and 8.

[19] River inflows do not contribute significantly to the water structure in the gulf, but local effects are apparent during both seasons, particularly during winter at Shatt Al Arab, north of the gulf (Figure 8). In addition, records show that precipitation during 1992 was very low in the gulf, so the relatively small fresh water inflow and the short period considered in this study (i.e., around 30 days each season) suggest that this is not likely to have had a significant impact on the dispersion mechanisms considered in this study.

4.3. Model Validation and Estimation of the Shear Scale

[20] The above information provided an excellent data set for the validation of the model hydrodynamics and associated dispersion. To optimize the test we carried out a 30 day simulation for both winter and summer configurations, with initial values as stated in Figure 2 (i.e., 13 May to 12 June 1992 and 27 January to 26 February 1992). The simulations were required to model first the hydraulic control across the Strait of Hormuz and fresh water input from the rivers, and then the dispersal of the salinity across the gulf, as observed in Figures 7 and 8. Evaluation of both temperature (mainly at the water surface) and salinity (mainly through the strait and rivers) provided the validation.

[21] The purpose of the validation simulations was to see whether ELCOM could reproduce the three-dimensional summer and winter temperature and salinity structures when forced with the data shown in Figures 3 and 4 and initialized with uniform water columns having values given as shown in Figure 2. The results from these simulations are shown here for the winter (Figures 9 and 11) and summer (Figures 10 and 12) periods; the agreement between the simulation results and the field data are generally excellent (Figures 9–12).

[22] During winter, relatively fresh water entered the gulf through the Strait of Hormuz, making its way to the comparatively deeper Iranian coast. In contrast, higher water densities were noticed all around the basin, particularly around the area surrounding Qatar and the UAE (Figure 9a, bottom). These results support the predominant control of

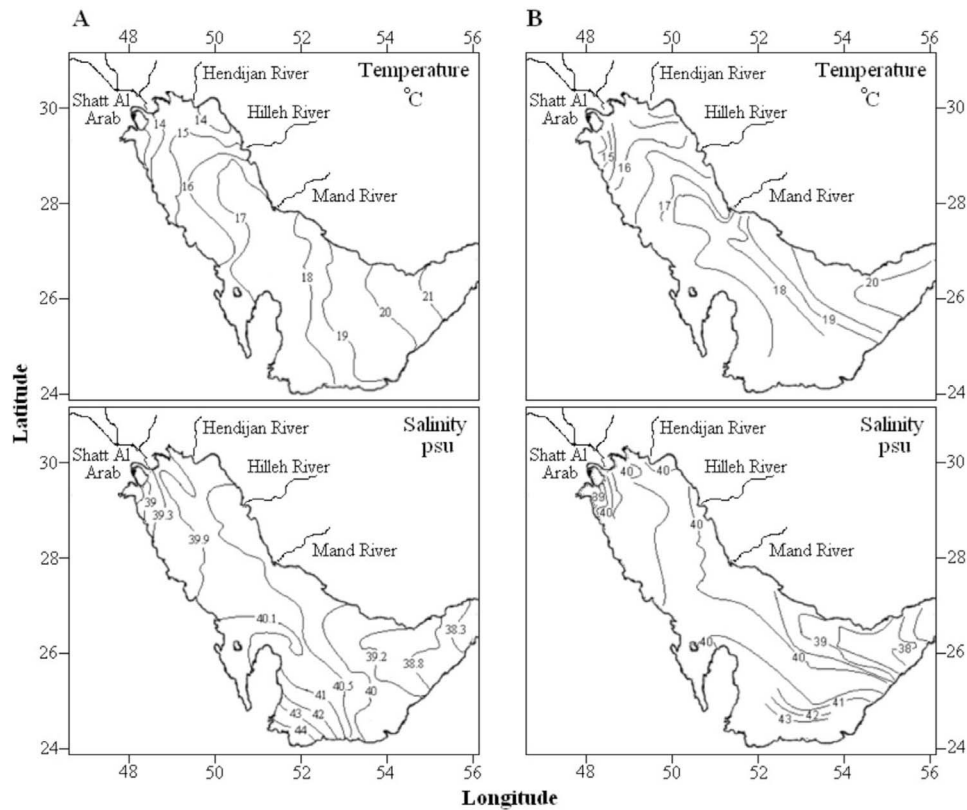


Figure 11. (a) Simulated surface variation of temperature and salinity of the gulf during winter. (b) Field data of temperature and salinity of the gulf during winter.

density by the salinity distribution (Figure 11a). This pattern is consistent with the broad circulation in the gulf where the Coriolis force deflects the surface inflow toward Iran and the subsurface outflow toward the Arabian coastline [Sultan *et al.*, 1995]. The salinity increased from 36 psu near the strait to 41 psu near Kuwait (Figures 9a, middle and 11), while the temperature fell from 22 to approximately 14°C, as shown in Figures 9a (top) and 11, at the same location. In the shallower waters of the gulf higher salinity levels are obvious, reaching 44 psu near the UAE coastal waters (Figure 11), resulting in an increase in the surface density and consequent vertical sinking (Figure 9a, bottom). This generally agreed with the findings of Reynolds [1993]. The simulations revealed that the gulf water is mostly mixed vertically along its main axis during 1992 winter conditions.

[23] Summer simulations exposed a more stratified structure in the estuary but with horizontal trends of both temperature and salinity similar to those of winter (Figures 10a, top and 10a, middle). A significant rise in water temperature of the estuary was evident parallel to the coastal areas of the gulf, as indicated in Figures 10a (top) and 12, reaching 31°C near the UAE. This sharp rise in temperature was due to the continuous heat input through the air-sea interface as indicated in Figure 4, leading to a rather lower surface water density than winter, ranging between 24 and 30 kg/m³ (Figure 10a, bottom). The contour plot in Figure 12 and the vertical plot in Figure 10 A imply that relatively cold, saline

and dense gulf water is found beneath the warmer, less saline and lighter surface inflow from the Gulf of Oman.

[24] As for the collected data, fresh water inflow from rivers did not significantly affect the flow characteristics of the basin as a whole for both seasons, but local effects were apparent, particularly at the far north of the gulf near Kuwait, where the Shatt Al Arab meets the hypersaline water (Figures 11 and 12). Also, during winter, at 650 km off the strait predictions in Figure 9a (middle) show salinity values (41 psu) lower than the summer 42 psu (Figure 10a, middle), suggesting that the river buoyancy effect is apparent in this region of the gulf.

[25] The scale of motion in the domain is shown in Figure 13, where the depth-averaged velocity of the spring flood tide at the Strait of Hormuz is depicted. Clearly the scale of the velocity field is considerably larger than the grid resolution of 5000 × 5000 m.

5. Geographic Distribution of Dispersion

5.1. Geographic Distribution of Dispersion Intensity

[26] Horizontal dispersion coefficients K_x were derived following Taylor [1954], Okubo [1971], and Lawrence *et al.* [1995] using

$$K_x = \frac{1}{4} \frac{\sigma^2}{t} \quad \text{and} \quad \sigma^2 = \frac{A_{90}}{7.23}$$

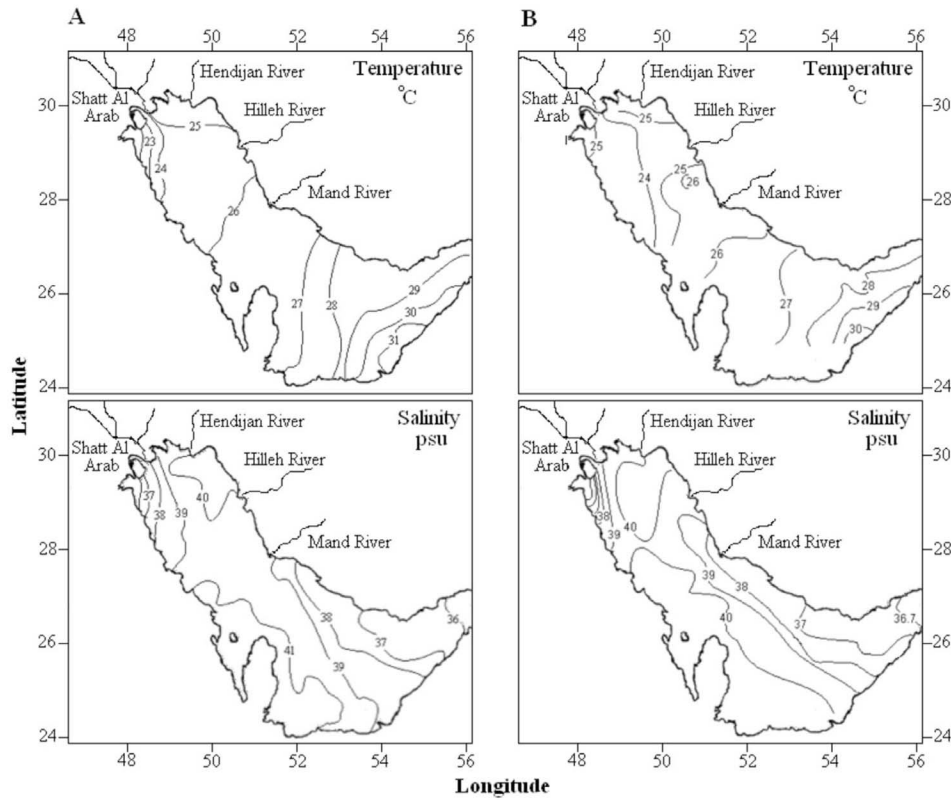


Figure 12. (a) Simulated surface variation of temperature and salinity of the gulf during summer. (b) Field data of temperature and salinity of the gulf during summer.

Here t is time (5, 20, and 40 days) and A_{90} is the horizontal area containing 90% of the tracer mass. The time for vertical mixing t_v can be estimated by arranging the above equation to give

$$t_v = \frac{\sigma_z^2}{4K_z}$$

It is usual to assume that vertical mixing is complete when the standard deviation equates to $0.8h$ [Lewis, 1997], where h is the total depth, and hence the mixing time is given by

$$t_v = \frac{(0.8h)^2}{4K_z} = \frac{0.32h^2}{K_z}$$

For a well-mixed estuary, a typical value of K_z would be $0.01 \text{ m}^2/\text{s}$ [Lewis, 1997], so that for a water depth of typically 36 m deep, such as the gulf, the above equations imply that $t_v = 5.75 \text{ h}$ for a complete mix scenario over the depth. Fischer et al. [1979] estimated the vertical mixing time scale to be

$$t_v = \frac{h^2}{10K_z}$$

Using similar values of K_z in the above equation, t_v is estimated to be 3.6 h.

[27] Horizontal dispersion coefficients were determined by observing the horizontal spread of four numerical tracers and utilizing the above equations. The numerical tracers

were introduced uniformly over the depth at various locations as shown in Figure 14, namely at stations T6, T7, T8, and T9. It is worth mentioning that the initial size of the patch was $5000 \times 5000 \text{ m}$, which equates to the size of a grid cell. The length scale was obtained by calculating $A_{90}/7.23$ using MATLAB, and the horizontal dispersion coef-

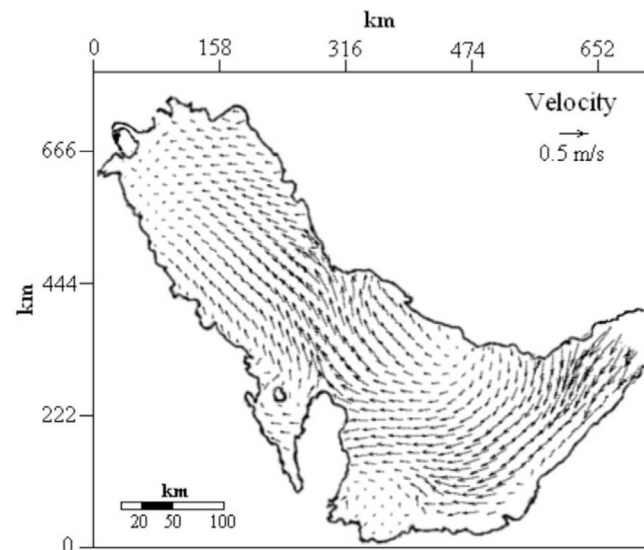


Figure 13. Depth-averaged velocity for spring flood tide during winter 1992 at the Strait of Hormuz.

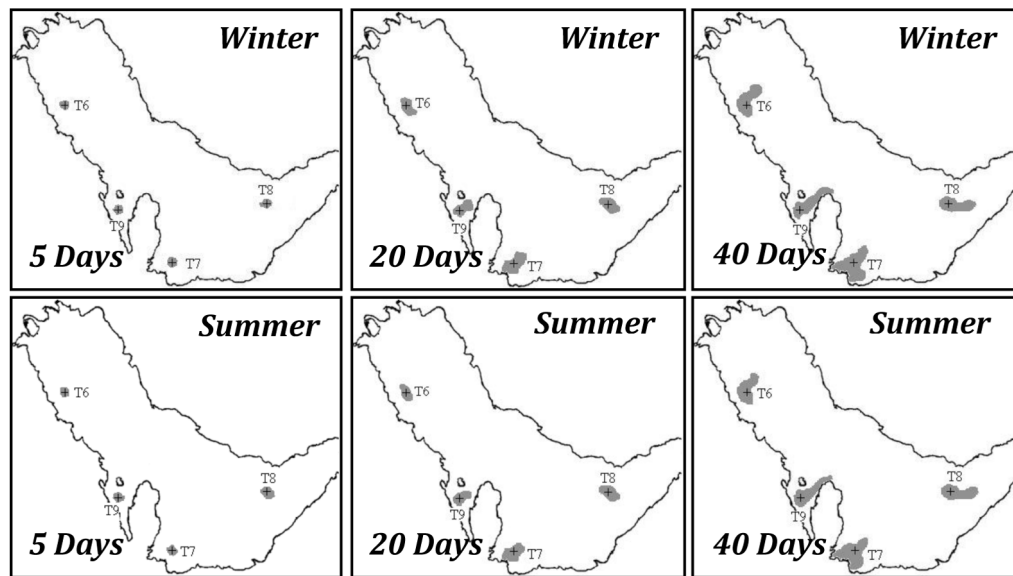


Figure 14. Tracer spread after 5, 20, and 40 days during summer and winter 1992, using meteorological effects from 18 January to 26 February for winter simulations and from 8 May to 12 June for summer simulations. Crosses indicate the release points.

ficient was calculated after 5, 20, and 40 days of continuous tracer release, starting from the validation period as in Table 1.

[28] In general, higher values were apparent near the Arabian coast. The highest dispersion coefficient occurred during winter, with a value of $141 \text{ m}^2/\text{s}$ at T9, during the early days of tracer release; similar values were achieved during summer. It is clear that even with higher horizontal diffusivities of 5 and $10 \text{ m}^2/\text{s}$, the dispersion coefficients remained almost the same as in Table 1. In the model validation section it was obvious that the effect of rivers was significant only locally, and buoyancy related to fresh water inflows would only be substantial in the long run. Hence the effect of rivers may be neglected since all locations of injections were far enough away from the fresh water inputs.

5.2. Residence Time

[29] Flushing time, age, and residence time are the commonly used measures for calculating retention characteristics of water or scalar quantities transported by the flow.

Boynton et al. [1995] argued that the residence time is a vital element that should be the basis of comparative analyses of ecosystem nutrient budgets. In practice, different approaches may lead to different time scales, even for the same domain [*Monsen et al.*, 2002].

[30] *Dronkers and Zimmerman* [1982] defined the residence time as the time taken for a whole water parcel to leave the lagoon through its outlet to the sea. In this study special attention was given to the residence time of the water in the whole estuary, since flushing time is an integrative system measure, whereas both residence time and age are local measures. In the case of the gulf, the circulation in and out of the Strait of Hormuz has been poorly defined in the past, resulting in estimates of the residence times varying widely from 2 to 5 years [*Hughes and Hunter*, 1979; *Hunter*, 1983]. *Sadrinasab and Kämpf* [2004] studied the flushing time of the gulf and found that 95% flushing times of surface waters ranged from 1 to 3 years along the Iranian coast, while larger values of more than 5 years were obtained along the Arabian coast.

Table 1. Dispersion Coefficients K_x (m^2/s) During Summer and Winter 1992^a

	5 Days			20 Days			40 Days		
	$\kappa = 1.0$	$\kappa = 5.0$	$\kappa = 10.0$	$\kappa = 1.0$	$\kappa = 5.0$	$\kappa = 10.0$	$\kappa = 1.0$	$\kappa = 5.0$	$\kappa = 10.0$
<i>Winter</i>									
T6	103	103	104	73	73	73	77	78	78
T7	99	99	100	86	86	86	90	90	90
T8	127	128	128	61	62	62	80	80	80
T9	140	141	141	87	88	88	83	83	83
<i>Summer</i>									
T6	100	100	100	70	71	71	75	75	76
T7	95	95	95	81	81	82	87	87	88
T8	126	127	127	60	61	61	83	83	83
T9	137	138	138	83	84	84	81	82	82

^aUsing meteorological effects from 18 January to 26 February for winter simulations and 8 May to 12 June for summer simulations, with $\kappa = 1, 5,$ and $10 \text{ m}^2/\text{s}$.

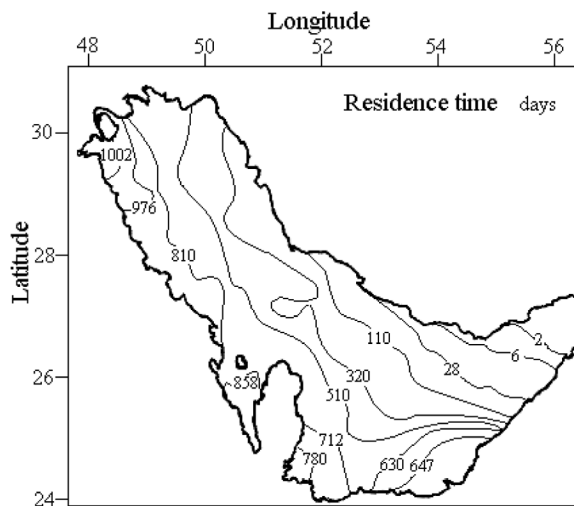


Figure 15. Residence time of the gulf in days.

[31] In modeling the residence time of the gulf using ELCOM, forcing model data of 1992 (January-December) were adopted and repeated for successive years. It was assumed that initially each cell contained water with a residence time of zero. The flushing time was defined as the residence time of the water as it left the domain (i.e., the time taken for the water to leave the domain). The model revealed that the residence time in the gulf was almost 3 years, as shown in Figure 15, the residence time being the longest time for water packages to remain along the Arabian coast of the gulf. In particular, near Kuwait Bay, Qatar and the UAE coast values reached 858 days. Obviously the residence time at the Strait of Hormuz was lowest (2 days), due to the open boundary effects in the region.

6. Discussion

[32] To determine the main drivers of the horizontal dispersion of the tracers various forcing scenarios were implemented for the sensitivity analysis. All the simulations were carried out using a selection of the above summer and winter forcing data from 1992, as detailed in Table 2.

[33] These simulations enabled a sensitive analysis to be undertaken for the various forcing mechanisms. As seen from Table 2, tidal forcing accounted for about two thirds of the total tracer dispersion at T6 and T7, almost 90% at T8 and 75% at T9 during summer and winter.

[34] Justification for using a 5000 m grid and the chosen horizontal diffusivity value is necessary before analyzing the

Table 2. Diffusion Coefficients (m^2/s) Due to Various Effects After 40 Days of Release

Experiment	Season	Tide	Wind	T6 (K_x)	T7 (K_x)	T8 (K_x)	T9 (K_x)
ELCOM1	Winter	Yes	No	49	60	69	60
ELCOM2	Winter	No	Yes	24	27	10	20
ELCOM3	Summer	Yes	No	53	60	72	60
ELCOM4	Summer	No	Yes	20	25	8	19

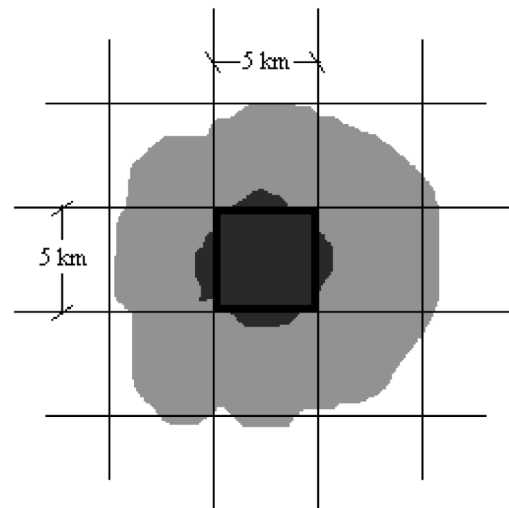


Figure 16. Injection of tracer at a representative cell, with a scale of 5000×5000 m, would typically take 30 days to spread 5000 m.

results obtained in this study. Previously, observations by Lawrence *et al.* [1995] suggested diffusivity values of $O(10^{-1}) \text{ m}^2/\text{s}$ for length scale of 500 m; also Stocker and Imberger [2003] computed turbulent diffusivities of $O(10^0) \text{ m}^2/\text{s}$ in Lake Kinneret. Okely *et al.* [2010] for Victoria Lake revealed that a horizontal diffusivity in ELCOM of less than $1 \text{ m}^2/\text{s}$ was appropriate. In this study, an initial horizontal diffusivity of $1 \text{ m}^2/\text{s}$ was utilized in the model, selected on the basis of Okubo's [1974] findings, in which a length scale of 5000 m corresponds to $1 \text{ m}^2/\text{s}$. By analogy, $1 \text{ m}^2/\text{s}$ would take account of horizontal dispersion at scales smaller than the model grid resolution as shown in Figure 16, in which this value is fixed throughout the simulation period. To ensure adequacy of the value chosen, the horizontal diffusivity was altered to $5 \text{ m}^2/\text{s}$ and then to $10 \text{ m}^2/\text{s}$ in the model, confirming that this did not significantly influence the horizontal dispersion of the tracers, as shown in Table 1. Therefore, Table 1 shows that as time progress the tracer at each station forms a circular patch during the first days after injection that eventually progresses into an oval shape along the mean flow direction due to turbulent diffusion, as shown in Figures 17a and 17b. However, as the patch size evolves due to further injection the oval shape is distorted and stretched, forming a random shape dependent on the direction of shear force effects and, to a smaller extent, large or small eddies. Shear effects playing the main role in expanding the patch size after 30 days will be explained in the following paragraph. It is worth mentioning that by using the Okubo [1974] K versus l graph to calculate K_x from the corresponding length scales of T6, T7, T8, and T9 during 20 days (shown in Table 1), values of 68, 78, 62, and $83 \text{ m}^2/\text{s}$ were obtained, with these values being similar to the respective computed values cited in Table 1.

[35] Scenarios adopted in this study and shown in Table 2 revealed that the gulf is mainly driven by tidal forces during both seasons and therefore tides are the main drivers in creating the shear forces that play key roles in dispersing the numerical tracers in both summer and winter. Although T8

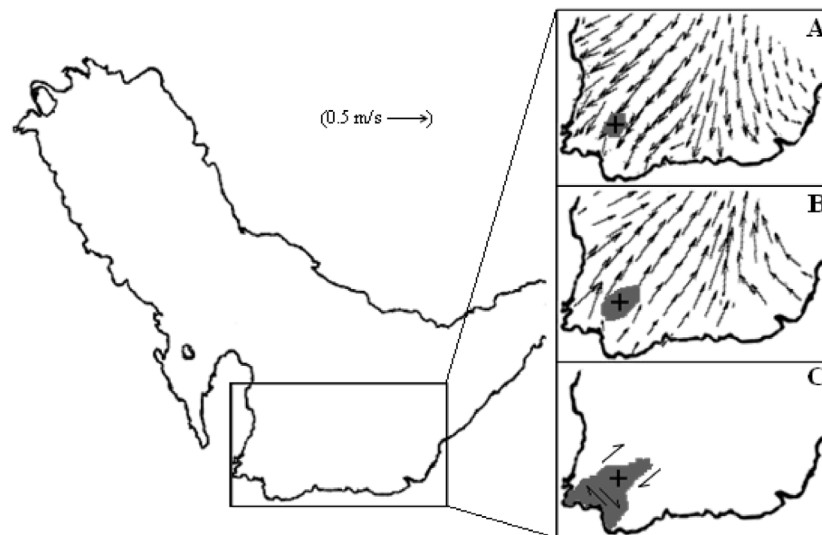


Figure 17. (a) Flood tide effect at T7 (5 days), (b) ebb tide effect at T7 (10 days), and (c) shear force effect in spreading the tracer at T7 (45 days).

was located at a site with a comparatively greater depth, the simulation suggests a dispersion coefficient similar to that at the shallower T6 site due to the uniform currents, since tracers spread out in both directions away from the release point, similar to the spread shown at T7 in Figures 17a and 17b. Furthermore, higher currents and consequently larger shear forces generated by tides are distinguishable and played a key role in dispersing the tracer at T8. Similarly, but to a smaller extent at T6, shear generated by wind speeds of approximately 15 m/s in a direction across the mean flow, combined with large eddies and Coriolis forces, enhanced dispersion by more than 15% along the estuary and deflected the patch in a seaward direction with dispersion coefficients comparable to values obtained at T8. Analogously, conditions at T9 are significantly affected by wind shear, but the topography at this location caused dispersion coefficients to be increased due to bed friction. This elongated the patch toward the north Qatar coastline, and eventually it became vulnerable to large eddies (e.g., Figure 13) as it developed toward the estuary main channel.

[36] At T7 the great contribution of tides in stretching the patch away from the release point toward the coast of the UAE and Qatar is indicated by its increase in size and developing a most random shape, as shown in Figure 17c. This can be explained by the combination of wind, tides, an irregular topography and coastal interaction that enhanced shear forces. Moreover, as the patch evolved, it interacted with the coastline, comprising of smaller bays and headlands that dramatically increased the dispersion coefficients after 40 days, giving rise to “Coastal Trapping” [Inoue and Wiseman, 2000] and making mixing efficient and chaotic (Figure 17c). Although the mixing processes appear to be considerable at T7, the residence time in Figure 15 suggests that the patch would prevail for about 750 days.

[37] Horizontal turbulent diffusion played a minor role because dispersion coefficients varied only slightly for different horizontal diffusivities (shown in Table 1). Bottom

and internal shear, as observed in the velocity profiles in the top center of the gulf, also contributed to vertical mixing of the water column particularly during summer due to minor stratification developing in the upper layer (Figure 10). Shear components of horizontal velocity along the Arabian coastline were greater both near the surface and near the bed, due to wind drift and bottom friction, respectively.

[38] The dispersion mechanisms affecting the gulf have a fundamental influence on the estuary ecology. Furthermore, spatial variability in the horizontal mixing and dispersion coefficients has several implications for water quality within the gulf. Due to the nature of the gulf, high nutrient values normally result in high rates of oxygen consumption, particularly in the relatively shallow Arabian shoreline [Brewer and Dyrssen, 1985], so dispersion processes arising from wind along this region would significantly influence the nutrient levels along the coast. Brewer and Dyrssen [1985] found high surface phosphorus levels that may be attributed to the vertical dispersion mechanism in such regions. Moreover, nutrient concentrations in the gulf have often been concentrated in the north of the gulf, in Kuwait Bay and in the region around the outfall of Shatt Al Arab, and they have been cited as the cause of a number of eutrophication incidents, mostly during summer. For example, a major red tide and an associated fish kill occurred in 1999 [Heil et al., 2001].

[39] An estimate of the fluid residence time, i.e., the average time a water particle spends within a region [Geyer and Signel, 1992], is given as

$$t_R = \frac{l^2}{K_x},$$

where $t_R \approx 200$ days for an average dispersion coefficient of $90 \text{ m}^2/\text{s}$ and $l = 40 \text{ km}$, an estimated length scale for the assemblage localities. This relatively long time scale allows the ecological niches to exist and promotes spatial hetero-

genity of biochemical material, in particular in the northern part of the gulf.

[40] **Acknowledgments.** The first author would like to thank CWR for financial support in enabling him to stay at the centre for 2 months. The authors would also like to acknowledge the Kuwait Institute of Scientific Research and Dubai Meteorological Office for providing meteorological data essential for this study. The manuscript benefited greatly from the editing of Allan Barton. This article represents Centre for Water Research reference ED 2318 YA.

References

- Aref, H. (1984), Stirring by chaotic advection, *J. Fluid Mech.*, 143, 1–21, doi:10.1017/S0022112084001233.
- Bowden, K. F. (1965), Horizontal mixing in the sea due to a shearing current, *J. Fluid Mech.*, 21, 83–95, doi:10.1017/S0022112065000058.
- Boylund, P. L., H. Aref, and M. A. Stremmer (2000), Topological fluid mechanics of stirring, *J. Fluid Mech.*, 403, 277–304, doi:10.1017/S0022112099007107.
- Boynton, W. R., J. H. Garber, R. Summers, and W. M. Kemp (1995), Input, transformations, and transport of nitrogen and phosphorus in Chesapeake Bay and selected tributaries, *Estuaries*, 18, 285–314, doi:10.2307/1352640.
- Brewer, P. G., and D. Dyrssen (1985), Chemical oceanography of the Persian Gulf, *Prog. Oceanogr.*, 14, 41–55, doi:10.1016/0079-6611(85)90004-7.
- Cartwright, D. E., and R. J. Tayler (1971), New computations of the tide-generating potential, *Geophys. J. R. Astron. Soc.*, 23, 45–73, doi:10.1111/j.1365-246X.1971.tb01803.x.
- Casulli, V., and E. Cattani (1994), Stability, accuracy and efficiency of a semi-implicit method for three-dimensional shallow water flow, *Comput. Math. Appl.*, 27, 99–112, doi:10.1016/0898-1221(94)90059-0.
- Casulli, V., and R. T. Cheng (1992), Semi-implicit finite difference methods for three dimensional shallow water flow, *Int. J. Numer. Methods Fluids*, 15, 629–648, doi:10.1002/flid.1650150602.
- Dooley, H. D., and J. H. Steele (1969), Wind driven currents near coast, *Ocean Dyn.*, 22, 213–223, doi:10.1007/BF02225162.
- Dronkers, J., and J. T. F. Zimmerman (1982), Some principles of mixing in tidal lagoons, *Oceanol. Acta*, 4, suppl., 107–117.
- Elshorbagy, W., M. H. Azam, and K. Taguchi (2006), Hydrodynamic characterization and modelling of the Arabian Gulf, *J. Waterw. Harbors Coastal Eng. Div. Am. Soc. Civ. Eng.*, 132, 47–56.
- Fischer, H. B., E. J. List, R. C. Y. Koh, J. Imberger, and N. H. Brooks (1979), *Mixing in Inland and Coastal Waters*, Academic, San Diego, Calif.
- Geyer, W. R., and R. P. Signel (1992), A reassessment of the role of tidal dispersion in estuaries and bays, *Estuaries*, 15, 97–108, doi:10.2307/1352684.
- Heil, C. A., P. M. Glibert, M. A. Al-Sarawi, M. Faraj, M. Behbehani, and M. Husain (2001), First record of a fish-killing *Gymnodinium* sp. bloom in Kuwait Bay, Arabian Sea: Chronology and potential causes, *Mar. Ecol. Prog. Ser.*, 214, 15–23, doi:10.3354/meps214015.
- Hodges, B. R., J. Imberger, A. Saggio, and K. B. Winters (2000), Modeling basin scale internal waves in a stratified lake, *Limnol. Oceanogr.*, 45, 1603–1620, doi:10.4319/lo.2000.45.7.1603.
- Hughes, P., and J. R. Hunter (1979), A proposal for a physical oceanography program and numerical modeling of the KAP region, *UNESCO Rep. Mar. Sci.* 27, Paris.
- Hunter, J. R. (1983), A review of the residual circulation and mixing processes in the KAP region, with reference to applicable modeling techniques, Oceanographic modeling of Kuwait Action Plan (KAP), *UNESCO Rep. Mar. Sci.* 28, Paris.
- Imberger, J., E. A. D. Mamouni, J. Anderson, M. L. Ng, S. Nicol, and A. Veale (2007), The index of sustainable functionality: A new adaptive, multicriteria measurement of sustainability—Application to Western Australia, *Int. J. Environ. Sustainable Dev.*, 6, 323–355, doi:10.1504/IJESD.2007.015309.
- Inoue, M., and W. J. Wiseman (2000), Transport, stirring and mixing processes in a Louisiana estuary: A model study, *Estuarine Coastal Shelf Sci.*, 50, 449–466, doi:10.1006/ecss.2000.0587.
- Laval, B. J., J. Imberger, B. R. Hodges, and R. Stocker (2003), Modeling circulation in lakes: Spatial and temporal variations, *Limnol. Oceanogr.*, 48, 983–994, doi:10.4319/lo.2003.48.3.0983.
- Lawrence, G. A., K. I. Ashley, N. Yonemitsu and J. R. Ellis (1995), Natural dispersion in a small lake, *Limnol. Oceanogr.*, 40, 1519–1526.
- Leonard, B. P. (1991), The ULTIMATE conservative difference scheme applied to unsteady one-dimensional advection, *Comput. Method. Appl. Mech. Eng.*, 88, 17–74, doi:10.1016/0045-7825(91)90232-U.
- Lewis, R. E. (1997), *Dispersion in Estuaries and Coastal Waters*, John Wiley, Chichester, U. K.
- Monsen, N. E., J. E. Cloern, L. V. Lucas, and S. G. Monismith (2002), A comment on the use of flushing time, residence time, and age as transport time scales, *Limnol. Oceanogr.*, 47, 1545–1553, doi:10.4319/lo.2002.47.5.1545.
- Newhouse, S., and T. Pignataro (1993), On the estimation of topological entropy, *J. Stat. Phys.*, 72, 1331–1351, doi:10.1007/BF01048189.
- Okely, P., J. Imberger, and K. Shimizu (2010), Particle dispersal due to interplay of motions in the surface layer of a small reservoir, *Limnol. Oceanogr.*, 55, 589–603, doi:10.4319/lo.2009.55.2.0589.
- Okubo, A. (1971), Oceanic diffusion diagrams, *Deep Sea Res.*, 18, 779–802.
- Okubo, A. (1974), Some speculations on oceanic diffusion diagrams, *Rapp. P.-V. Reun. Cons. Int. Explor. Mer.*, 167, 77–85.
- Reynolds, R. M. (1992a), Report of activities—Leg I of the Mt. Mitchell Expedition, *Rep. HMRAD 92–9*, NOAA, Seattle, Wash.
- Reynolds, R. M. (1992b), Report of activities—Leg VI, A/B of the Mt. Mitchell Expedition, *Rep. HMRAD 92–10*, NOAA, Seattle, Wash.
- Reynolds, R. M. (1993), Physical oceanography of the gulf, Strait of Hormuz, and the Gulf of Oman—Results from Mt. Mitchell expedition, *Mar. Pollut. Bull.*, 27, 35–59, doi:10.1016/0025-326X(93)90007-7.
- Richardson, L. F. (1926), Atmospheric diffusion shown on a distance-neighbour graph, *Proc. R. Soc. London A*, 110, 709–737, doi:10.1098/rspa.1926.0043.
- Richlen, M. L., et al. (2010), The catastrophic 2008–2009 red tide in the Arabian Gulf region, with observations on the identification and phylogeny of the fish-killing dinoflagellate *Cochlodinium polykrikoides*, *Harmful Algae*, 9, 163–172, doi:10.1016/j.hal.2009.08.013.
- Sadrinasab, M., and J. Kämpf (2004), Three-dimensional flushing times of the Persian Gulf, *Geophys. Res. Lett.*, 31, L24301, doi:10.1029/2004GL020425.
- Spigel, R. H., J. Imberger, and K. N. Rayner (1986), Modeling the diurnal mixed layer, *Limnol. Oceanogr.*, 31, 533–556, doi:10.4319/lo.1986.31.3.0533.
- Stocker, R., and J. Imberger (2003), Horizontal transport and dispersion in the surface layer of a medium-sized lake, *Limnol. Oceanogr.*, 48, 971–982, doi:10.4319/lo.2003.48.3.0971.
- Sultan, S. A. R., F. Ahmad, N. M. El-Ghribi, and A. M. Al-Subhi (1995), An analysis of the Arabian Gulf monthly mean sea level, *Cont. Shelf Res.*, 15, 1471–1482, doi:10.1016/0278-4343(94)00081-W.
- Taylor, G. I. (1954), The dispersion of matter in turbulent flow through a pipe, *Proc. R. Soc. London A*, 223, 446–468.

Y. Alosairi and R. A. Falconer, Cardiff School of Engineering, Cardiff University, Queen's Building, The Parade, Cardiff CF24 3AA, UK. (alosauriy@cf.ac.uk)

J. Imberger, Centre for Water Research, University of Western Australia, M023, 35 Stirling Hwy., Crawley, WA 6009, Australia.